Biochimica et Biophysica Acta 1848 (2015) 2414–2421

Contents lists available at ScienceDirect

Biochimica et Biophysica Acta

journal homepage: www.elsevier.com/locate/bbamem

Comparative study of the mechanism of action of the antimicrobial peptide gomesin and its linear analogue: The role of the β-hairpin structure

Tatiana M. Domingues, Katia R. Perez, Antonio Miranda, Karin A. Riske *

Departamento de Biofísica, Escola Paulista de Medicina, Universidade Federal de São Paulo, R. Pedro de Toledo 669, L9D, CEP 04039-032 São Paulo, SP, Brazil

ARTICLE INFO

Article history:
Received 19 May 2015
Received in revised form 8 July 2015
Accepted 21 July 2015
Available online 29 July 2015

Keywords:
Antimicrobial peptide
Gomesin
Model membranes
ITC
Vesicle aggregation

ABSTRACT

Gomesin (Gm) is an antimicrobial peptide first isolated from the hemolymph of a Brazilian spider. Its powerful antimicrobial activity is, however, accompanied by hemolysis. As an alternative to this issue, a linear analogue (named GmL) lacking the disulfide bonds was designed. Here, CD spectroscopy, a fluorescence-based leakage assay, isothermal titration calorimetry (ITC) and light scattering are used to study the interaction of both Gm and GmL with large unilamellar vesicles (LUVs) composed of POPC (palmitoyl oleoyl phosphatidylcholine) with 25 and 50 mol% POPG (palmitoyl oleoyl phosphatidylglycerol). The activities of Gm and GmL in respect to their binding affinity/enthalpy, ability to permeabilize membranes and to induce vesicle aggregation are correlated with peptide secondary structure. Whereas Gm displays a quite stable β-hairpin motif irrespective of the environment, GmL assumes a random conformation in aqueous solution and in the presence of 25 mol% POPG but adopts a β-like structure in the presence of 50 mol% POPG. Gm exhibited high lytic activity against both surface charge densities. Instead, the activity of GmL was found to be negligible in the presence of 25 mol% POPG LUVs, but comparable to that of the native peptide against 50 mol% POPG as a consequence of peptide structuring. We conclude that the activity of Gm and its linear analogue is intimately related to the formation of a β-turn motif, in which the hydrophobic residues form a hydrophobic face able to insert into the membrane and disrupt it.

1. Introduction

Antimicrobial peptides are molecules of the immune defense system of animals and plants that play an important role in protection against pathogenic agents, such as bacteria and fungi [1–4]. Their mode of action generally depends on permeabilization and/or rupture of the cell membrane of microorganisms. They generally exhibit a broad spectrum of action, suggesting that the binding to target microbial cells is not mediated by receptors [5]. Despite the structural diversity of these molecules, they commonly exhibit an amphipathic character with a positive net charge [6–9], features that are essential to allow them to bind to the membrane of microorganisms, which is rich in anionic lipids [10–12]. Different lytic mechanisms have been proposed to elucidate peptide-induced membrane permeabilization/rupture, such as the toroidal pore mechanism, in which peptides and lipids stabilize pores across the membrane, and the carpet mode of action, in which peptides cover the membrane ultimately leading to its disruption [13]. Additionally, it has been proposed that some antimicrobial peptides might exert their activity after formation of amyloid-like fibers in the membrane [14,15]. Antimicrobial peptides have been largely studied because of their potential use as a new class of antibiotics [16,17]. First isolated from the innate immune system of different organisms [18], they can be chemically synthesized and modified, aiming at the improvement of their antimicrobial activity and reduction of hemolysis [19]. Since the lytic mechanism of antimicrobial peptides generally rely on unspecific interactions with membrane lipids, model membranes have been widely used to unravel the mechanisms underlying peptide/membrane interactions [20–25].

Gomesin (Gm) is a powerful antimicrobial peptide present in hemocytes of the Brazilian spider *Acanthoscurria gomesiana*. It consists of 18 amino acid residues (pGlu^{1}-Cys-Arg-Arg-Leu^{5}-Cys-Tyr-Lys-Gln-Arg^{10}-Cys-Val-Thr-Tyr-Cys^{15}-Arg-Gly-Arg-NH_2) with six positive charges. Four cysteine residues (Cys^{2,15} and Cys^{6,11}) confer to this peptide a β-hairpin conformation in aqueous solution, as described by Mandard et al. based on NMR studies [26]. Gm was first isolated and characterized in 2000 by Silva et al. in a pioneer study that demonstrated the Gm ability to kill bacteria and fungi with low minimum inhibitory concentrations (MICs) [27]. Besides the antimicrobial activity, Gm was related to apoptosis, inducing Ca^{2+} influx in mammalian cells and in tumor cell line CHO [28,29]. However, Gm also exhibits a relatively high hemolytic activity. This hemolytic effect could be reduced or even abolished if specific modifications were done in the peptide structure. The removal of

* Corresponding author.
E-mail address: kariske@unifesp.br (K.A. Riske).

http://dx.doi.org/10.1016/j.bbamem.2015.07.012
0005-2736/

both disulfide bonds, as for instance in the analogue [$Ser^{2,6,11,15}$]-Gm (termed hereafter GmL), resulted in a significant decrease in the peptide hemolytic activity [19,30]. Even though the MICs found for GmL were higher than those of Gm, its therapeutic index (defined for each pathogen as the ratio between peptide concentration that caused 10% hemolysis and the peptide MIC) is better than that of Gm. Yet, this analogue was rapidly degraded when incubated in human serum. Fázio et al. [19,30] showed previously that Gm structure is not changed by the solvent, whereas linear analogues can adopt secondary structures according to the environment. Working with different analogues of Gm, Moraes et al. [31] studied the interaction of these peptides with SDS (sodium dodecyl sulfate) micelles and their antimicrobial activity. The results emphasize the importance of the β-hairpin structure of Gm for its biological activity.

In a previous study, we used optical microscopy to study the interaction of Gm and its linear analogue GmL with giant unilamellar vesicles (GUVs) composed of palmitoyl-oleoylphosphatidylcholine (POPC) and palmitoyl-oleoylphosphatidylglycerol (POPG), in different molar ratios [32]. We showed that both Gm and GmL induce sudden burst of GUVs, suggesting a carpet mode of action [33,34]. The activity of GmL was found to be significantly lower than that of Gm for low POPG fraction, but becomes comparable to that of Gm for high POPG content. In recent works, we studied the interaction of Gm and different analogues that preserve the β-hairpin conformation with large unilamellar vesicles (LUVs) composed of POPC and POPG using different approaches, namely isothermal titration calorimetry (ITC), leakage of a fluorescent probe entrapped in vesicles and light scattering measurements [35,36]. ITC data showed that binding of Gm to anionic membranes is an exothermic process that follows a stoichiometry of roughly one gomesin charge per lipid charge. Light scattering data show that Gm binding is always accompanied by peptide-induced lipid aggregation [35]. This phenomenon is not exclusive for Gm, and it was reported for other antimicrobial peptides [37,38]. Comparative studies of the activity of Gm with analogues with different hydrophobic/hydrophilic balance and peptide charge showed that the magnitude of the enthalpy change measured with ITC and the leakage percentage induced are mainly governed by peptide hydrophobicity [36]. On the other hand, peptide charge is decisive in defining the extension of aggregation. Gm and analogues containing a Trp residue were also able to interact with SDS molecules [39].

In the present work, we perform a comprehensive study to compare the activity of Gm with that of its linear analogue GmL, which lacks the disulfide bonds. LUVs composed of POPC with 25 and 50 mol% POPG are used as model membranes to study the effect of membrane negative charge on the activity of both peptides, which have the same six positive charges. Circular dichroism, a leakage assay, ITC, light scattering and zeta potential measurements are used to investigate the activity and mode of action of Gm and GmL. These methods have been traditionally used to study the interaction of model membranes with different antimicrobial peptides [40–43]. We show that the activity of Gm is very high against both membrane compositions explored, whereas the activity of GmL is strongly modulated by the fraction of POPG in the membrane.

2. Material and methods

2.1. Material

The lipids 1-palmitoyl-2-oleoyl-sn-glycero-3-phosphocholine (POPC), 1-palmitoyl-2-oleoyl-sn-glycero-3-phospho-(1′-rac-glycerol) (sodium salt) (POPG) were purchased from Avanti Polar Lipids (Birmingham, AL). The fluorescent probe 5(6)-carboxyfluorescein (CF), the detergent Triton X-100, the buffer HEPES and NaCl were purchased from Sigma-Aldrich (St. Louis, MN, USA). CF was purified before use as described previously [44].

2.2. Peptide synthesis, purification and characterization

Gm and GmL were synthesized by the solid phase method [45], using a MBAR (methylbenzhydrylamine) resin, and employing the *t*-Boc strategy. After cleavage of the peptides from the resin, Gm was submitted to a disulfide bond formation process monitored by liquid chromatography coupled to a mass spectrometer, while GmL was directly purified. The purifications of the peptides from lyophilized crude solutions were done by high performance liquid chromatography (HPLC) in a C_{18} column. To guaranty high purity and to characterize both peptides, HPLC coupled to a mass spectrometer (MS) was used. Peptide purity was also assessed by amino acid analysis (AAA), performed by ion-exchange chromatography on a Beckman 6300 amino acid analyzer (Fullerton, CA). The results are listed in Table S1 in the Supplementary material. At the end, the concentrations of Gm and GmL were assessed by the optical density of the tyrosine and cystine residues, when present, at $\lambda = 280$ nm [46].

2.3. Preparation of large unilamellar vesicles (LUVs)

A lipid film of the desired composition (POPC with 25 or 50 mol% POPG) was formed on the walls of a test tube from a lipid stock solution in chloroform, dried with a stream of N_2 and kept in a vacuum for 2 h. The lipid film was resuspended in a buffer solution (30 mM HEPES, pH 7.4, containing 100 mM NaCl if not stated otherwise), and vortexed to form multilamellar vesicles (MLVs). This lipid dispersion was extruded at least 11 times through a polycarbonate membrane with a pore size of 100 nm to yield LUVs.

For carboxyfluorescein (CF) leakage assay, LUVs were prepared in 30 mM HEPES, pH 7.4, containing 50 mM CF and 86 mM glucose. Glucose was added to adjust the osmolarity of the solution. After the extrusion as described above, the lipid dispersion was filtered through a Sephadex resin G-25 medium column using 30 mM HEPES with 100 mM NaCl as eluting buffer to remove free CF. LUVs with entrapped CF were collected from the void volume of the column.

To verify the phospholipid concentration at the end of the extrusion process, a method based on the indirect determination of phosphorous content was employed [47].

2.4. Circular dichroism (CD)

CD spectra were acquired using a Jasco spectropolarimeter (J-810, Japan), in the range of 190–250 nm. The mixture of peptide (100 μM) and lipid (500 μM) was placed in a circular quartz cuvette of 0.5 mm light path. For the CD measurements, the samples were prepared in 10 mM phosphate buffer, pH 7.4, since 30 mM HEPES buffer and chloride ions absorbs strongly at or below 200 nm, interfering with CD bands [48]. The acquisition parameters used were: 4 s response time, 50 nm/min speed acquisition, 0.2 nm step in 4 accumulations. All experiments were done at room temperature. The final spectra, in millidegree (θ), were expressed in units of residue molar ellipticity, $[\theta]_{MRW}$ (deg cm^2 $dmol^{-1}$), according to: $[\theta]_{MRW} = (\theta * MRW) / (\ell * c * 10)$, where MRW is the mean residue weight (protein mean weight/number of residues), ℓ is the optical length (cm) and c is the peptide concentration (mg/mL).

2.5. Carboxyfluorescein (CF) leakage assay

CF leakage experiments were performed in a Hitachi spectrofluorometer (F-2500, Washington, DC). A quartz cuvette of 1 cm light path was filled with 0.5 mL of a suspension of LUVs (50 μM lipid concentration) containing 50 mM CF entrapped (CF-LUVs), as described above. The CF fluorescence was monitored at $\lambda = 520$ nm, using $\lambda = 490$ nm as excitation wavelength. Different concentrations of peptides (0.05–10 μM) were added to CF-LUV suspension. At the end of the experiment (~55 min), 10 μL of Triton X-100 at 10% (w/v) were added to promote

total CF leakage from LUVs. The CF leakage percentage was calculated using the following equation: %Leakage = $100(F_t - F_0) / (F_{max} - F_0)$, where F_0 is the CF fluorescence before peptide addition, F_t is the CF fluorescence at the chosen time, and F_{max} is the CF fluorescence after detergent addition [35].

2.6. Isothermal titration calorimetry (ITC)

A microcalorimeter VP-ITC from Microcal (Northampton, MA) was used to assess the thermodynamic parameters of lipid–peptide interaction. For this, the calorimeter cell (1.4576 mL) was filled with the peptide solution, and the syringe was loaded with a dispersion of LUVs. Lipid aliquots of 5 μL were injected into the peptide solution every 10 min. A first 0.5 μL injection was always made to reduce the volumetric error of the syringe plunger and discarded from the analysis. The temperature was set to 25 °C.

2.7. Static light scattering

Measurements of 90° static light scattering were done in a Hitachi spectrofluorometer (F-2500) in the same conditions as the ITC experiments. A peptide solution was placed in a quartz cuvette of 1 cm light path (1.5 mL), and sequential 5 μL injections of LUVs from a stock solution were done every 10 min. All experiments were performed at room temperature and under magnetic stirring.

2.8. Zeta potential and dynamic light scattering

Dynamic light scattering (DLS) and electrophoretic mobility (using laser Doppler velocimetry) measurements were performed with a Zetasizer Nano ZS (Malvern, UK). Both measurements were done after sequential injections from a 300 μM peptide stock solution in a cuvette containing LUVs at 0.1 mM lipid concentration. For these measurements, 100 mM NaF was used instead of NaCl to reduce oxidation of the electrodes, since the fluoride redox potential is higher than that of chloride and hardly reached by the voltage potential applied by the equipment. The DLS data are given as the Z-average particle size as a function of the peptide-to-lipid molar ratio. Zeta potential, ζ, was calculated from the measured electrophoretic mobility (μ) using the Henry equation: $\zeta = \frac{3\eta\mu}{2\varepsilon f(\kappa a)}$, where ε is the dielectric constant and η the water viscosity; f(ka) in this case is 1.5, referring to the Smoluchowski approximation.

3. Results and discussion

The interaction of the antimicrobial peptide gomesin (Gm) and its linear analogue [$Ser^{2,6,11,15}$]-Gm (GmL) with negatively charged LUVs was studied with different experimental approaches. The LUVs were composed of POPC containing either 25 or 50 mol% POPG to explore the role of membrane negative charge in the activity of the cationic peptides. In the following, the results obtained with each technique are presented separately.

3.1. CD measurements

The conformation of Gm and GmL was evaluated by circular dichroism (CD) both in buffer solution and in the presence of LUVs at a 0.2 peptide-to-lipid (P/L) molar ratio. This high P/L was chosen since both peptide and lipid concentrations have a strict range of variation: at lower peptide concentrations the CD signal is very weak or absent, and at higher lipid concentrations the CD signal is noisy, due to increased sample turbidity. The CD spectra are shown in Fig. 1. The CD spectra of Gm in buffer and in the presence of LUVs (curves in black) are characteristic of a β-hairpin structure, as previously described by Mandard et al. using the NMR technique [26]. A small red shift in the negative band (~2 nm) is observed in the presence of 50 mol% POPG.

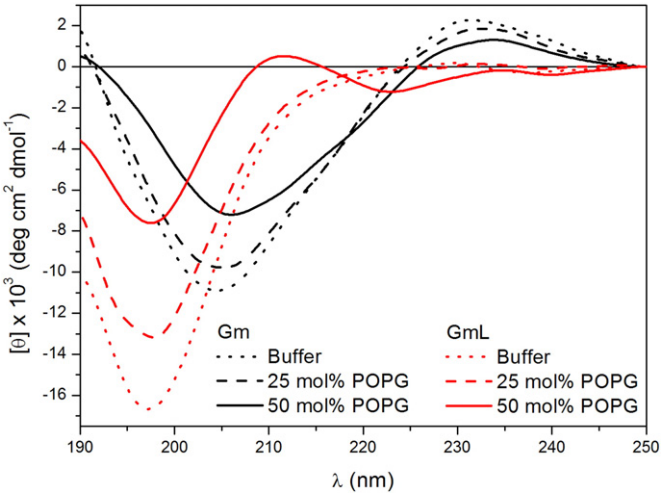

Fig. 1. Circular dichroism spectra of 100 μM Gm and GmL in buffer (dotted lines), and in the presence of LUVs of POPC with 25 (dashed lines) and 50 mol% POPG (solid lines) (500 μM lipid concentration).

The linear analogue GmL, which lacks the disulfide bonds that confer the β-hairpin structure to Gm, showed spectrum features of a random motif with a negative band at ~198 nm in buffer solution (red dotted line in Fig. 1), as expected [19]. The conformation of GmL is almost unaltered in the presence of LUVs composed of 25 mol% POPG (red dashed line). However, by increasing the POPG content of the LUVs to 50 mol%, the CD spectrum (red straight line) of GmL acquires two new bands: a positive at ~211 nm and a negative at ~223 nm. The last negative band is present in peptides that adopt a β-turn motif, with the positive band around 205 nm [49]. When the content of POPG was increased up to 100 mol% (Fig. S1), the negative band around 223 nm became more evident, and the positive band was shifted to ~197 nm, corresponding to a well-defined turn II spectrum, while Gm adopts a turn I motif [49]. Even though the CD spectra of GmL in the presence of LUVs are different from those of Gm, they display feature characteristic of β-structures. This shows that GmL has a tendency to adopt β-structures instead of α-helix in the presence of negatively charged bilayers. The percentages of secondary structures obtained from data fits are shown in the Supplementary material (Table S2).

3.2. CF leakage assay

The ability of Gm and GmL to permeabilize membranes was monitored by the leakage of the fluorescent probe CF, initially entrapped in LUVs in high concentration (50 mM) with self-quenched fluorescence. Peptide-induced leakage is detected as an increase in the fluorescence intensity, which can be directly related to the percentage of CF leakage (Section 2.5).

CF leakage kinetics induced by Gm and GmL in LUVs of 25 and 50 mol% POPG were obtained at five different peptide-to-lipid molar ratios in the range 0.001–0.2 P/L. All curves obtained are shown in the Supplementary material (Fig. S3) and the ones for the highest P/L tested are shown in Fig. 2A. The CF leakage induced by both Gm and GmL in 50 mol% POPG occurs very fast and reaches almost full leakage within a few seconds. The native peptide also induces high leakage percentage in 25 mol% POPG, but at a much slower rate. This difference in kinetic mechanism was observed for all P/L ratios tested (see Fig. S3). Instead, only a mild leakage is induced by the linear analogue in 25 mol% POPG.

Fig. 2B shows the percentage of CF leakage reached at the end of the experiment (~55 min) as a function of P/L. For most conditions, this time was enough to reach a roughly constant maximal leakage value.

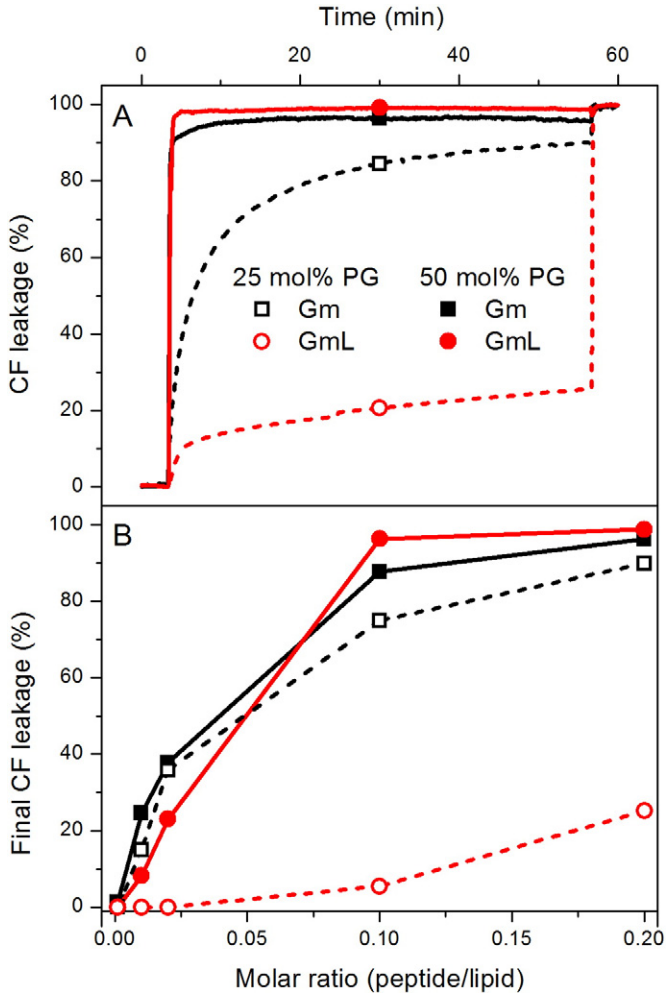

Fig. 2. CF leakage from LUVs. A) Kinetics of the percentage of CF leakage from LUVs of POPC with 25 (open symbols and dashed lines) and 50 mol% POPG (solid symbols and solid lines) in the presence of Gm (black) and GmL (red) at 0.2 P/L molar ratio. Addition of the peptide occurred after 3 min and a concentrated aliquot of Triton X-100 was added close to the end of the experiment (~55 min) to induce full leakage. B) Percentage of CF leakage at ~55 min as a function of the peptide-to-lipid molar ratio. The percentage of leakage was calculated based on the equation described in Material and methods.

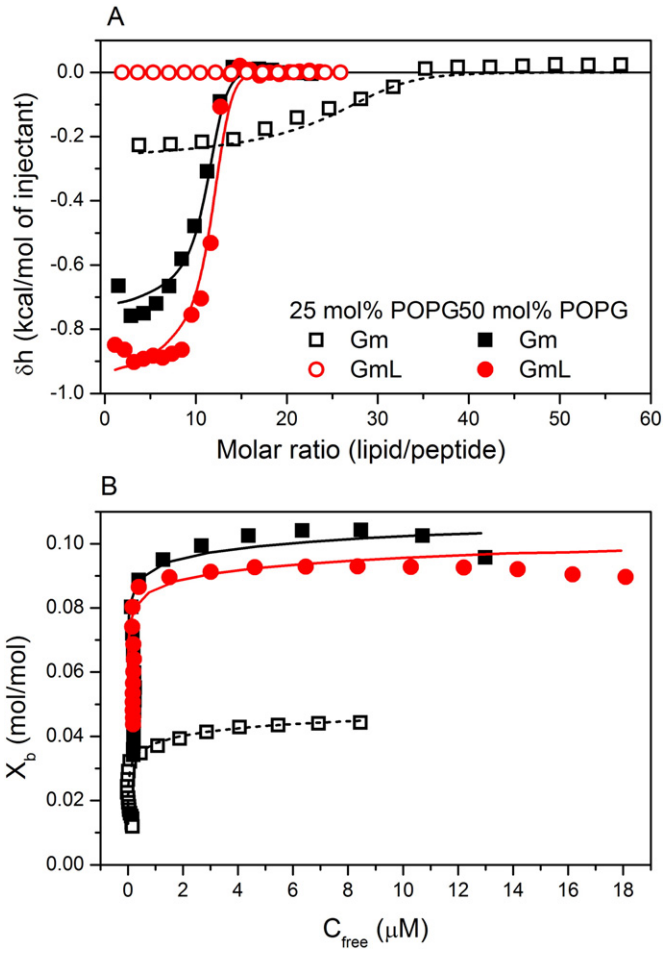

Fig. 3. ITC data obtained from the titration of Gm (black) and GmL (red) with LUVs composed of POPC with 25 (open symbols) and 50 mol% POPG (solid symbols). The experimental data is represented by symbols, showing A) the integrated heat per mole of injectant, δh, as a function of the lipid-to-peptide molar ratio, and B) the binding isotherms (extent of binding X_b as a function of the concentration of free peptide C_{free}). The lines refer to the best fit obtained with the surface partition model combined with the Gouy–Chapman theory (the fit parameters are listed in Table 1). Peptide concentration in cell was 10 μM (25 mol% POPG) and 15 μM (50 mol% POPG) Gm, and 20 μM GmL. The lipid concentration used was 10 (25 mol% POPG) and 6 mM (50 mol% POPG). The injection volume used was 5 μL. Buffer: HEPES 30 mM with 100 mM NaCl, pH 7.4. The temperature was 25 °C.

The lytic activity of Gm is basically the same for both membrane compositions tested, reaching almost complete leakage at the highest P/L. Similar behavior was observed for the activity of GmL against 50 mol% POPG. On the other hand, GmL induced low CF leakage from LUVs of 25 mol% POPG.

3.3. Isothermal titration calorimetry (ITC)

ITC experiments were performed as a titration of the peptide solution with LUVs. The heat flow curves as a function of time and the heat per mole of injectant, δh, obtained from the integration of each peak, are shown in the Supplementary material (Fig. S4). Fig. 3A shows δh as a function of the lipid-to-peptide molar ratio (L/P) for all conditions explored. The interaction of Gm with charged LUVs is mainly an exothermic process, with and inflection point corresponding roughly to 6 PG/Gm, i.e., one negative lipid charge per positive charge of Gm. The same trend is detected in the interaction of GmL with 50 mol% POPG. However, no detectable interaction was found between the linear analogue and 25 mol% POPG. The total ΔH of the process (obtained by summing the δh along the titration and dividing by the number of moles of peptides in the calorimeter cell) is shown in Table 1.

Fig. 3B shows the binding isotherms (extent of peptide binding per mole of lipid, X_b, as a function of the concentration of free peptide available, C_{free}) calculated from the ITC data (see ref. [36] for details). In the

Table 1
Thermodynamic parameters obtained from ITC experiments of Gm and GmL with 25 and 50 mol% POPG LUVs.

	ΔH (kcal/mol)	K (M^{-1})	TΔS (kcal/mol)
25 mol% POPG			
Gm	−5.6	1×10^4	+2.2
GmL	0	–	
50 mol% POPG			
Gm	−7.0	5×10^5	+3.1
GmL	−9.4	1×10^5	−0.2

ΔH is the reaction heat per mole of peptide and K is the intrinsic binding constant in the surface partition model combined with the Gouy–Chapman theory. The effective charge of the peptides was +5.5. The entropic contribution, TΔS, was calculated from the thermodynamic relations $\Delta G = \Delta H - T\Delta S$ and $\Delta G = -RT \ln (55.5\ K)$, where the term 55.5 corrects the unit of K to molar fraction.

beginning of the ITC titration (high C_{free}), the binding isotherms show the maximum extent of peptide binding per lipid (in excess of peptide). If these values are given with respect to POPG only (see Fig. S5 in the Supplementary material), the following P_{bound}/POPG values are obtained: 0.20, 0.19 and 0.18, representing again almost one lipid charge per peptide charge. The binding isotherms obtained for each system exhibit different details, but the overall trend is the same and is mainly dictated by a charge–charge interaction.

The ITC data were fit with a surface partition model combined with the Gouy–Chapman theory, as described in detail elsewhere [35,41,50]. This model describes the membrane/water partition of cationic peptides at charged interfaces taking into account the Boltzmann distribution created by the membrane surface potential. The fits were done using the experimental value of ΔH and fixing the effective charge of Gm and GmL to $z = +5.5$, very close to the nominal charge of both peptides. The total lipid concentration was taken into account, since from leakage experiments (Fig. 2), almost complete leakage is detected in the L/P range along the titration curve, implying that all lipids are available for binding. The only free parameter left was the intrinsic binding constant, K. The best fits obtained with this model are shown as lines in Fig. 3 and the corresponding thermodynamic parameters obtained are shown in Table 1. The binding constant K and ΔH of Gm are higher for the more charged surface. The fact that these parameters are sensitive to the membrane charge density shows that the model used is not perfect in describing peptide–lipid interaction. Nevertheless, we can still conclude that Gm and structured GmL interact with anionic lipids mainly in a one-to-one charge fashion and in an enthalpy-driven process which can be associated with a non-classical hydrophobic effect upon insertion of the hydrophobic face into the membrane [36,50].

The interaction parameters obtained for Gm and GmL with 50 mol% POPG are similar, but the enthalpy change of GmL is higher than that of Gm. This higher ΔH can be partially explained by the structuring of GmL upon binding to the membrane surface. Considering that one GmL molecule could make up to five H-bonds, according to the structure adopted by native Gm [26], and that each H-bond contributes with ΔH ~ 0.3 kcal/mol [51,52], the change in GmL conformation from disordered to β-turn could account for an additional ΔH in the range of 1.5 kcal/mol. An entropic contribution was detected only for the binding of Gm, which is probably associated with the loss of hydration water molecules as the peptide binds to and inserts its hydrophobic region into the membrane. This contribution in the linear analogue is probably compensated by the peptide structuring at the membrane interface.

3.4. Light scattering measurements

Static and dynamic light scattering assays were done to monitor the lipid aggregation promoted by Gm and GmL. Static light scattering measurements (Fig. 4) were set to reproduce the same experimental conditions as those of the ITC experiments (Fig. 3). The dotted lines in black refer to the light scattering intensity obtained from lipid injection into a buffer solution, for which a constant value dependent on the lipid concentration is obtained. Injections of LUVs into a peptide solution show a quite different outcome, depending on membrane charge and the peptide. Mild aggregation is detected as an increased light scattering, as observed for the titration of GmL with LUVs of 25 mol% POPG (Fig. 4A, red). When micrometer-sized aggregates are formed, light scattering initially increases sharply and then decreases due to precipitation of the aggregates (see e.g. black curves in Fig. 4A). This effect is even stronger for injections of 50 mol% POPG LUVs into Gm or GmL (Fig. 4B). The extensive aggregation pattern is detected for the same injections that give rise to exothermic signals in the ITC experiment (see Fig. 3). After that, constant light scattering with time is observed, showing that no further aggregation occur.

Dynamic light scattering (DLS) data were acquired by titration of a dispersion of LUVs with peptide. The titration was performed in a reverse way as compared with ITC and static light scattering measurements to monitor the effect of the peptides on the initial size and zeta potential (next section) of LUVs. Fig. 5 shows the Z-average size obtained when LUVs were titrated with Gm and GmL. The sizes of the LUVs of 25 mol% POPG remain roughly constant at their original size (~100 nm) during the titration with GmL. In all other cases, a significant increase in size up to micrometers is observed. DLS measurements are not accurate for such large size aggregates, resulting in large fluctuations in the Z-average values at high P/L molar ratios. The onset of aggregation depends mainly on membrane composition and is consistent with the different stoichiometry detected in the ITC experiment. Micrometer-sized aggregates are also reached around 6 PG/peptide.

The light scattering results show that binding of both Gm and GmL to charged LUVs is always accompanied by lipid aggregation. The extent of aggregation is highly enhanced by membrane charge and correlates with peptide binding/affinity. Since Gm has its six positive charges distributed around the β-hairpin structure [26], it becomes easier for Gm to interact with adjacent LUVs [36]. On the other hand, the ability of the linear analogue GmL to induce aggregation depends on its acquiring a secondary structure similar to that of Gm. The peptide–lipid aggregates proposed to be formed are depicted as a model in ref. [23], with the peptides linking adjacent bilayers or even creating bulk phase patches in which a bilayer structure no longer exists.

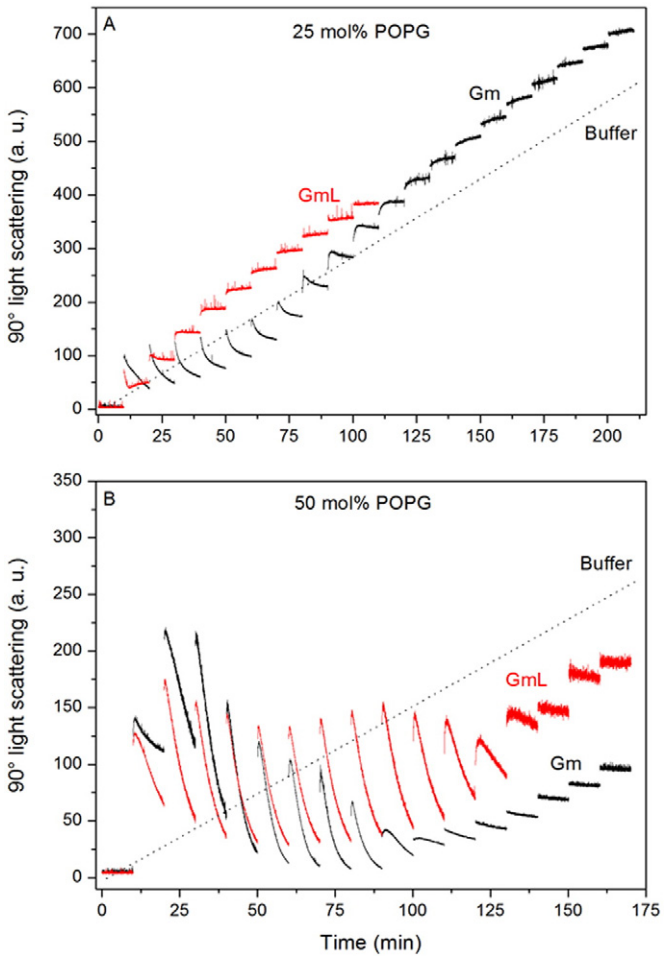

Fig. 4. 90° light scattering measurements (λ = 600 nm) obtained from lipid injections (5 μL) into a peptide solution. The L/P ratio of each injection corresponds to those of the ITC experiment (Fig. 3) for each condition. A) Titration of 10 μM Gm (black lines) and 20 μM GmL (red lines) with LUVs of POPC with 25 mol% POPG (10 mM), and B) titration of 15 μM Gm (black lines) and 20 μM GmL (red lines) with LUVs of POPC with 50 mol% POPG (6 mM). The buffer titration with LUVs for both conditions is presented as a dashed line (black) in each graph.

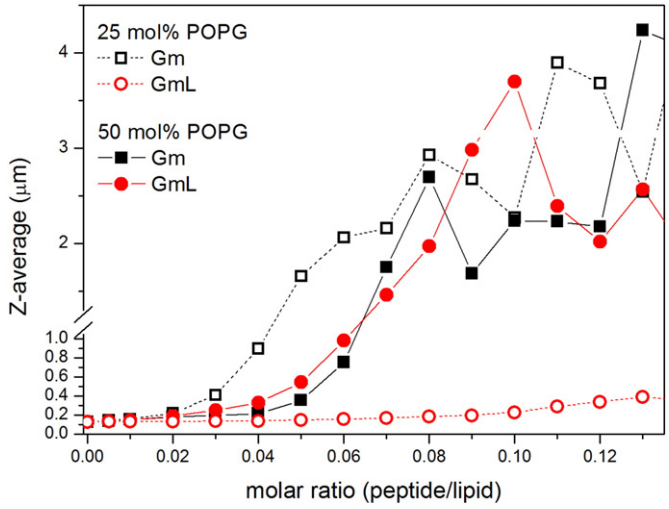

Fig. 5. Dynamic light scattering of Gm (data in black) and GmL (data in red) interacting with LUVs composed of POPC with 25 (dashed lines and open symbols) and 50 mol% POPG (solid lines and solid symbols). The Z-average of particles (μm) is presented as a function of the peptide-to-lipid molar ratio.

3.5. Zeta potential measurements

Zeta potential was calculated from electrophoretic mobility measurements (Section 2.8) along the titration of LUVs with Gm and GmL, in the same titration experiment in which the DLS results were obtained. The results are shown in Fig. 6. The initial value, at P/L = 0, was obtained in the absence of peptide. The zeta potential becomes less negative with the addition of peptides, indicating binding of the cationic peptides to the anionic membrane surface. Complete charge neutralization is seen only for Gm with 50 mol% POPG above 0.1 P/L. Charge reversal would not be expected since from the ITC binding curves (see Fig. 3B) the maximum peptide bound per mole of lipid is slightly lower than complete charge neutralization. However, it should be stressed that micrometer-sized aggregates are formed and precipitate in all conditions except for 25 mol% POPG in the presence of GmL (see Figs. 4 and 5). The dashed lines in Fig. 6 indicate the P/L above which micrometer-sized aggregates were detected with DLS. Up to that point, the data can be trusted and show a similar trend as observed with the other techniques. The zeta potential is only slightly affected by the addition of GmL to 25 mol% POPG, whereas it becomes significantly less negative upon the addition of GmL to 50 mol% POPG and of Gm to both membrane compositions. Above the P/L ratio indicated with the dashed lines, the data obtained from addition of Gm and GmL to 50 mol% POPG diverge significantly, probably an artifact due to the extent of aggregation.

4. Conclusions

The interaction of the antimicrobial peptide Gm and its linear analogue GmL with charged LUVs was assessed with complementary approaches to provide a comprehensive picture of the mechanism of action of Gm focusing the role of peptide secondary structure and membrane charge. Peptide activity was correlated with its ability to bind to and permeabilize membranes and to induce vesicle aggregation. In a general view, all techniques showed that the activity of Gm is much higher than that of GmL at low membrane surface charge (25 mol% POPG), but their activities become practically the same at high POPG content (50 mol% POPG). These results agree well with our previous work with giant unilamellar vesicles (GUVs) in the presence of Gm and GmL [32].

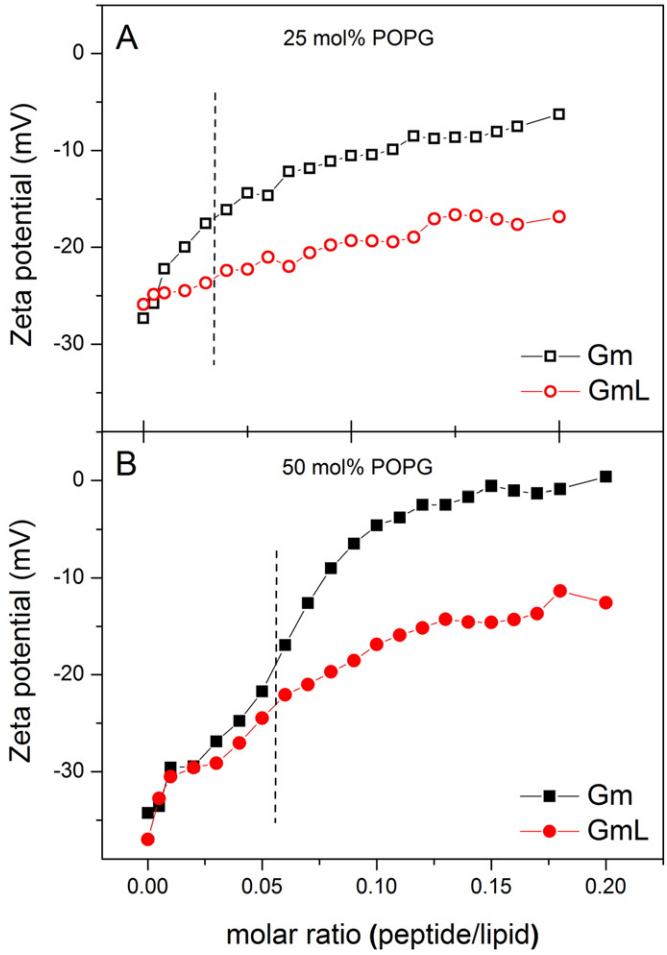

Fig. 6. Zeta potential (ζ) measurements for Gm (black) and GmL (red) interacting with LUVs composed of POPC with A) 25 (open symbols) and B) 50 mol% POPG (solid symbols) as a function of the peptide-to-lipid molar ratio. The dashed lines indicate the P/L molar ratio above which micrometer-sized aggregates were detected with DLS (Fig. 5) performed on the same sample.

In the conditions explored in the present study, the conformations adopted by Gm and GmL at the membrane interface, as assessed by CD data, are directly related to peptide activity. Gm, which due to the disulfide bonds adopts a quite stable β-hairpin structure irrespective of the environment, exhibited high activity toward 25 and 50 mol% POPG. On the other hand, the activity of the linear analogue GmL was strongly modulated by membrane surface charge. LUVs containing 25 mol% POPG, with a low density of negative charges, would favor a more relaxed conformation of GmL. At higher POPG density, GmL adopts a β-turn conformation in which the hydrophobic residues (Leu^5, Tyr^7, Val^{12} and Tyr^{14}) form an apolar face able to insert into and perturb the membrane, in a similar way as Gm [26,36]. Fig. 7 shows structures of Gm and GmL consistent with their CD spectra in different environments (see Supplementary material for further details). GmL adopts the active conformation in the presence of highly charged membranes. Taking into account that the membrane of some microorganisms exhibits a high fraction of charged lipids, a linear version of Gm could show a promising therapeutic window combining low hemolysis with high antimicrobial activity against such pathogens.

Transparency document

The Transparency Document associated with this article can be found, in the online verison.

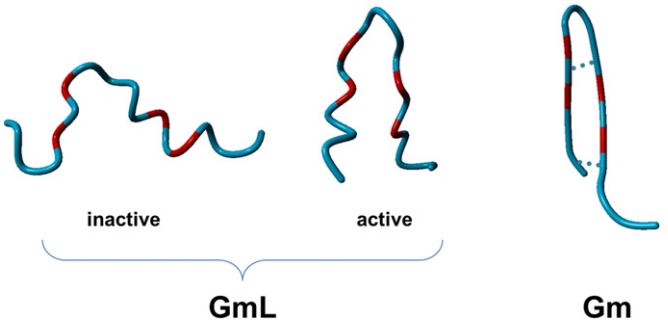

Fig. 7. Structures of Gm and GmL drawn with the program YASARA view [53] from PDB structures. The backbones are shown in blue and the hydrophobic residues (Leu^5, Tyr^7, Val^{12} and Tyr^{14}) are colored with red. The conformations of GmL were obtained from structure predictions using the online software I-TASSER [54–56]. The theoretical CD spectra of these structures are shown in Fig. S3 and are similar to the experimental spectra of GmL in buffer (inactive) and in the presence of 75 mol% POPG (active). The structure of Gm (ID: 1kfp, [57]) corresponds to the one reported by Mandard et al. [26]. The dotted lines represent the disulfide bonds.

Acknowledgments

The financial support of FAPESP (2012/10442-8, 2009/54558-7), CNPq (472054/2011-2), and INCT-FCx (573560/2008-0, 2008/57685-7) is acknowledged. We are thankful to Dr. Joachim Seelig for allowing us to use the ITC analysis program developed by his group. We thank Bruno Mattei for the help with drawing the structures of Gm and GmL.

Appendix A. Supplementary data

Supplementary data to this article can be found online at http://dx.doi.org/10.1016/j.bbamem.2015.07.012.

References

[1] M. Zasloff, Antimicrobial peptides of multicellular organisms, Nature 415 (2002) 389–395.
[2] H. Jenssen, P. Hamill, R.E.W. Hancock, Peptide antimicrobial agents, Clin. Microbiol. Rev. 19 (2006) 491–511.
[3] L.T. Nguyen, E.F. Haney, H.J. Vogel, The expanding scope of antimicrobial peptide structures and their modes of action, Trends Biotechol. 29 (2011) 464–472.
[4] Y. Shai, Mode of action of membrane active antimicrobial peptides, Peptide Science 66 (2002) 236–248.
[5] M.R. Yeaman, N.Y. Yount, Mechanisms of antimicrobial peptide action and resistance, Pharmacol. Rev. 55 (2003) 27–55.
[6] G. Laverty, S.P. Gorman, B.F. Gilmore, The potential of antimicrobial peptides as biocides, Int. J. Mol. Sci. 12 (2011) 6566–6596.
[7] W.C. Wimley, Describing the mechanism of antimicrobial peptide action with the interfacial activity model, ACS Chem. Biol. 5 (2010) 905–917.
[8] M. Lerch-Bader, C. Lundin, H. Kim, I. Nilsson, G. von Heijne, Contribution of positively charged flanking residues to the insertion of transmembrane helices into the endoplasmic reticulum, Proc. Nat. Acad. Sci. USA 105 (2008) 4127–4132.
[9] Z. Jiang, A.I. Vasil, L. Gera, M.L. Vasil, R.S. Hodges, Rational design of α-helical antimicrobial peptides to target gram-negative pathogens, *Acinetobacter baumannii* and *Pseudomonas aeruginosa*: utilization of charge, 'specificity determinants', total hydrophobicity, hydrophobe type and location as design parameters to improve the therapeutic ratio, Chem. Biol. Drug Des. 77 (2011) 225–240.
[10] R.M. Epand, H.J. Vogel, Diversity of antimicrobial peptides and their mechanisms of action, Biochim. Biophys. Acta 1462 (1999) 11–28.
[11] A.T.Y. Yeung, S.L. Gellatly, R.E.W. Hancock, Multifunctional cationic host defence peptides and their clinical applications, Cell. Mol. Life Sci. 68 (2011) 2161–2176.
[12] L.M. Yin, M.A. Edwards, J. Li, C.M. Yip, C.M. Deber, Roles of hydrophobicity and charge distribution of cationic antimicrobial peptides in peptide–membrane interactions, J. Biol. Chem. 287 (2012) 7738–7745.
[13] K.A. Brogden, Antimicrobial peptides: pore formers or metabolic inhibitors in bacteria? Nat. Rev. Microbiol. 3 (2005) 238–250.
[14] G.P. Gorbenko, P.K.J. Kinnunen, The role of lipid–protein interactions in amyloid-type protein fibril formation, Chem. Phys. Lipids 141 (2006) 72–82.
[15] A.K. Mahalka, P.K.J. Kinnunen, Binding of amphipathic α-helical antimicrobial peptides to lipid membranes: lessons from temporins B and L, Biochim. Biophys. Acta 1788 (2009) 1600–1609.
[16] J. Wang, E.S.W. Wong, J.C. Whitley, J. Li, J.M. Stringer, K.R. Short, M.B. Renfree, K. Belov, B.G. Cocks, Ancient antimicrobial peptides kill antibiotic-resistant pathogens: Australian mammals provide new options, PLoS One 6 (2011) (e24030).
[17] Z. Li, X. Xu, L. Meng, Q. Zhang, L. Cao, W. Li, Y. Wu, Z. Cao, Hp1404, a new antimicrobial peptide from the scorpion *Heterometrus petersii*, PLoS One 9 (2014) (e97539).
[18] J. Théolier, I. Fliss, J. Jean, R. Hammami, MilkAMP: a comprehensive database of antimicrobial peptides of dairy origin, Dairy Sci. & Technol. 94 (2014) 181–193.
[19] M.A. Fázio, L. Jouvensal, F. Vovelle, P. Bulet, M.T. Miranda, S. Daffre, A. Miranda, Biological and structural characterization of new linear gomesin analogues with improved therapeutic indices, Biopolymers 88 (2007) 386–400.
[20] L. Zhang, A. Rozek, R.E.W. Hancock, Interaction of cationic antimicrobial peptides with model membranes, J. Biol. Chem. 276 (2001) 35714–35722.
[21] A.A. Stromstedt, L. Ringstad, A. Schmidtchen, M. Malmsten, Interaction between amphiphilic peptides and phospholipid membranes, Curr. Opin. Colloid Interface Sci. 15 (2010) 467–478.
[22] J. Wang, M. Mura, Y. Zhou, M. Pinna, A.V. Zvelindovsky, S.R. Dennison, D.A. Phoenix, The cooperative behaviour of antimicrobial peptides in model membranes, Biochim. Biophys. Acta 1838 (2014) 2870–2881.
[23] K.A. Riske, Optical microscopy of giant vesicles as a tool to reveal the mechanism of action of antimicrobial peptides and the specific case of gomesin, Adv. Planar Lipid Bilayers Liposomes 21 (2015) 99–129.
[24] P.F. Almeida, A. Pokorny, Mechanisms of antimicrobial, cytolytic, and cell-penetrating peptides: from kinetics to thermodynamics, Biochemistry 48 (2009) 8083–8093.
[25] A.N. McKeown, J.L. Naro, L.J. Huskins, P.F. Almeida, A thermodynamic approach to the mechanism of cell-penetrating peptides in model membranes, Biochemistry 50 (2011) 654–662.
[26] N. Mandard, P. Bulet, A. Caille, S. Daffre, F. Vovelle, The solution structure of gomesin, an antimicrobial cysteine-rich peptide from the spider, Eur. J. Biochem. 269 (2002) 1190–1198.
[27] P.I. Silva Jr., S. Daffre, P. Bulet, Isolation and characterization of gomesin, an 18-residue cysteine-rich defense peptide from the spider *Acanthoscurria gomesiana* hemocytes with sequence similarities to horseshoe crab antimicrobial peptides of the tachyplesin family, J. Biol. Chem. 275 (2000) 33464–33470.
[28] M.V. Buri, T.M. Domingues, E.J. Paredes-Gamero, R.L. Casaes-Rodrigues, E.G. Rodrigues, A. Miranda, Resistance to degradation and cellular distribution are important features for the antitumor activity of gomesin, PLoS ONE 8 (2013) 80924.
[29] E.J. Paredes-Gamero, R.L. Casaes-Rodrigues, G.E.D.D. Moura, T.M. Domingues, M.V. Buri, V.H.C. Ferreira, E.S. Trindade, A.J. Moreno-Ortega, M.F. Cano-Abad, H.B. Nader, A.T. Ferreira, A. Miranda, G.Z. Justo, I.L.S. Tersariol, Cell-permeable gomesin peptide promotes cell death by intracellular Ca^{2+} overload, Mol. Pharmaceutics 9 (2012) 2686–2697.
[30] M.A. Fázio, V.X. Oliveira Jr., P. Bulet, M.T. Miranda, S. Daffre, A. Miranda, Structure–activity relationship studies of gomesin: importance of the disulfide bridges for conformation, bioactivities, and serum stability, Biopolymers 84 (2006) 205–218.
[31] L.G.M. Moraes, M.A. Fázio, R.F.F. Vieira, C.R. Nakaie, M.T.M. Miranda, S. Schreier, S. Daffre, A. Miranda, Conformational and functional studies of gomesin analogues by CD, EPR and fluorescence spectroscopies, Biochim. Biophys. Acta 1768 (2007) 52–58.
[32] T.M. Domingues, K.A. Riske, A. Miranda, Revealing the lytic mechanism of the antimicrobial peptide gomesin by observing giant unilamellar vesicles, Langmuir 26 (2010) 11077–11084.
[33] E.E. Ambroggio, F. Separovic, J.H. Bowie, G.D. Fidelio, L.A. Bagatolli, Direct visualization of membrane leakage induced by the antibiotic peptides: maculatin, citropin, and aurein, Biophys. J. 89 (2005) 1874–1881.
[34] Y. Tamba, M. Yamazaki, Single giant unilamellar vesicle method reveals effect of antimicrobial peptide magainin 2 on membrane permeability, Biochemistry 44 (2005) 15823–15833.
[35] T.M. Domingues, B. Mattei, J. Seelig, K.R. Perez, A. Miranda, K.A. Riske, Interaction of the antimicrobial peptide gomesin with model membranes: a calorimetric study, Langmuir 29 (2013) 8609–8618.
[36] B. Mattei, A. Miranda, K.R. Perez, K.A. Riske, Structure-activity relationship of the antimicrobial peptide gomesin: the role of peptide hydrophobicity in its interaction with model membranes, Langmuir 30 (2014) 3513–3521.
[37] A. Ziegler, X.L. Blatter, A. Seelig, J. Seelig, Protein transduction domains of HIV-1 and SIV TAT interact with charged lipid vesicles. Binding mechanism and thermodynamic analysis, Biochemistry 42 (2003) 9185–9194.
[38] E. Gonçalves, E. Kitas, J. Seelig, Binding of oligoarginine to membrane lipids and heparan sulfate: structural and thermodynamic characterization of a cell-penetrating peptide, Biochemistry 44 (2005) 2692–2702.
[39] T.M. Domingues, M.V. Buri, S. Daffre, P.T. Campana, K.A. Riske, A. Miranda, Structure–activity relationship of Trp-containing analogs of the antimicrobial peptide gomesin, J. Pept. Sci. 20 (2014) 421–428.
[40] J.T.J. Cheng, J.D. Hale, M. Elliot, R.E.W. Hancock, S.K. Straus, Effect of membrane composition on antimicrobial peptides aurein 2.2 and 2.3 from Australian southern bell frogs, Biophys. J. 96 (2009) 552–565.
[41] T. Wieprecht, M. Beyermann, J. Seelig, Binding of antibacterial magainin peptides to electrically neutral membranes: thermodynamics and structure, Biochemistry 38 (1999) 10377–10387.
[42] G. Klocek, T. Schulthess, Y. Shai, J. Seelig, Thermodynamics of melittin binding to lipid bilayers. Aggregation and pore formation, Biochemistry 48 (2009) 2586–2596.
[43] S. Rex, G. Schwarz, Quantitative studies on the melittin-induced leakage mechanism of lipid vesicles, Biochemistry 37 (1998) 2336–2345.
[44] E. Ralston, L.M. Hjelmeland, R.D. Klausner, J.N. Weinstein, R. Blumenthal, Carboxyfluorescein as a probe for liposome–cell interactions effect of impurities, and purification of the dye, Biochim. Biophys. Acta 649 (1981) 133–137.

[45] A. Miranda, S.C. Koerber, J. Gulyas, S.L. Lahrichi, A.G. Craig, A. Corrigan, A. Hagler, C. Rivier, W. Vale, J. Rivier, Conformationally restricted competitive antagonists of human/rat corticotropin-releasing factor, J. Med. Chem. 37 (1994) 1450–1459.
[46] A. Aitken, M. Learmonth, Protein determination by UV absorption, in: J.M. Walker (Ed.), The Protein Protocols Handbook, Human Press Inc. 1996, pp. 3–6.
[47] G. Rouser, S. Fkeischer, A. Yamamoto, Two dimensional then layer chromatographic separation of polar lipids and determination of phospholipids by phosphorus analysis of spots, Lipids 5 (1970) 494–496.
[48] S.M. Kelly, T.J. Jess, N.C. Price, How to study proteins by circular dichroism, Biochim. Biophys. Acta 1751 (2005) 119–139.
[49] G.D. Fasman, Circular Dichroism and the Conformational Analysis of Biomolecules, Plenum Press, New York, 1996.
[50] M.R. Wenk, J. Seelig, Magainin 2 amide interaction with lipid membranes: calorimetric detection of peptide binding and pore formation, Biochemistry 37 (1998) 3909–3916.
[51] W.C. Wimley, S.H. White, Reversible unfolding of β-sheets in membranes: a calorimetric study, J. Mol. Biol. 342 (2004) 703–711.
[52] M. Meier, J. Seelig, Thermodynamics of the coil ⇆ β-sheet transition in a membrane environment, J. Mol. Biol. 369 (2007) 277–289.
[53] E. Krieger, G. Vriend, YASARA view—molecular graphics for all devices—from smartphones to workstations, Bioinformatics 30 (2014) 2981–2982.
[54] J. Yang, R. Yan, A. Roy, D. Xu, J. Poisson, Y. Zhang, The I-TASSER suite: protein structure and function prediction, Nature Methods 12 (2015) 7–8.
[55] A. Roy, A. Kucukural, Y. Zhang, I-TASSER: a unified platform for automated protein structure and function prediction, Nature Protocols 5 (2010) 725–738.
[56] Y. Zhang, I-TASSER server for protein 3D structure prediction, BMC Bioinformatics 9 (2008) 40.
[57] PDB ID: 1kfp. N. Mandard, P. Bulet, A. Caile, S. Daffre, F. Vovelle, The solution structure of gomesin, an antimicrobial cysteine-rich peptide from the spider, Eur. J. Biochem. 269 (2002) 1190–1198.